Korean J. Chem. Eng., **21**(6), 1153-1160 (2004)

Numerical Methodology for Proton Exchange Membrane Fuel Cell Simulation using Computational Fluid Dynamics Technique

Chi Seung Lee and Sung Chul Yi†

Department of Chemical Engineering, Hanyang University, Seoul 133-791, Korea
(*Received 28 June 2004 • accepted 8 November 2004*)

Abstract−To analyze the physical phenomena occurring in the Proton Exchange Membrane Fuel Cell (PEMFC) using Computational Fluid Dynamics (CFD) technique under an isothermal operating condition, four major governing equations such as continuity equation, momentum conservation equation, species transport equation and charge conservation equation should be solved. Among these governing equations, using the interfacial boundary condition is necessary for solving the water transport equation properly since the concept of water concentration in membrane/electrode assembly (MEA) and other regions is totally different. It was first attempted to solve the water transport equation directly in the MEA region by using interfacial boundary condition; and physically-meaningful data such as water content, proton conductivity, etc. were successfully obtained. A detailed problem-solving methodology for PEMFC is presented and result comparison with experimental data is also implemented in this paper.

Key words: PEMFC, CFD, Modeling

INTRODUCTION

The Proton Exchange Membrane Fuel Cell (PEMFC) is a kind of generator that produces electricity through electro-chemical reactions. Since, unlike a battery, it requires fuel gases for generating electricity, there are several transport phenomena (e.g., fluid convection, species transport, heat transfer, etc.) in fuel cell [Carrette et al., 2000, 2001; Larminie et al., 2000]. Besides, there are mainly three electro-chemical reactions in the anode and cathode catalyst layer such as hydrogen oxidation reaction, oxygen reduction reaction, water generating reaction. In order to numerically simulate these phenomena, five major governing equations such as continuity, momentum conservation, energy conservation, species transport and charge conservation equation should be solved simultaneously. However, since isothermal operating condition is assumed in this paper, the energy conservation equation is currently out of our research focus.

In Finite Volume Method (FVM) based computational fluid dynamics (CFD) technique, it is unnecessary to give interfacial boundary conditions since the solver gradually approaches to get the converged numerical solutions by balancing flux values in each control volume with external information, the so-called boundary condition. So, while using FVM-based CFD technique, we do not have to consider internal boundary conditions for the reason mentioned above.

However, when PEMFC is given as a target system, the situation is quite different. This is due to complex physical phenomena in PEMFC. In general systems, physical phenomena are usually continuous through the entire computational domain. However, when it comes to PEMFC, phenomena inside PEMFC are not continuous: (i) hydrogen, oxygen and water vapor distribution discontinuity, (ii) liquid water distribution discontinuity (exists only in MEA), and (iii) electrolyte potential distribution discontinuity. To deal with this phenomenally discontinuous problem, several numerical techniques (e.g. source term maximizing) were used in other researches.

However, even with these numerical techniques, it is nearly impossible to deal with water transport phenomenon in MEA since boundary conditions between gas diffusion layer and catalyst layer are required. This is because the concept of mass (or mole) fraction of water membrane is inexplicable--to paraphrase, the value of the mass fraction in the membrane always has to be unity since only water vapor exists in that region. So, though water status in MEA is not exactly determined, solving the water concentration equation in the MEA region is necessary in order to get physically-reasonable proton conductivity.

Dutta et al. [2000] and Berning et al. [2002] solved mass fraction-based species transport equations and dealt with water species as a gas phase. They did not consider the MEA region as a computational domain; in other words, governing equations were not solved in the MEA region. Only the catalyst layer was considered as a face (not as a volume) source because of its thickness.

Um et al. [2000] solved the whole computational domain including the MEA region with a single domain concept. However they did not solve the water concentration profile in MEA; instead, they solved the water vapor species transport equation to get water activity values in MEA. In order to obtain the water content values in MEA they used the experimental relationship between water activity and water content that Springer et al. [1999] had presented. They used the linear extrapolation method to predict water content value in a range that water activity is over unity. This is phenomenally inexplicable since the water activity value is always equal to or less than unity. Also, the water vapor mass fraction value in the membrane region is physically inexplicable since only one species (water vapor) exists in the MEA region, i.e., the common concept of mass fraction cannot be used in MEA.

In PEMFC modeling, water content is one of the most important key factors in predicting current density distribution in MEA

†To whom correspondence should be addressed.
E-mail: scyi@hanyang.ac.kr

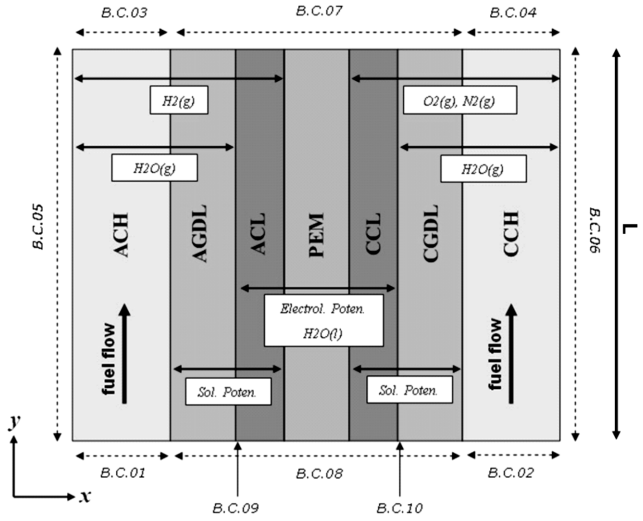

Fig. 1. A Schematic of PEM fuel cell.

since proper and physically-understandable water content values give exact electrolyte potential distribution in MEA. Consequently, current density distribution is calculated by using this electrolyte potential gradient.

From this point of view, water content prediction should be based on water concentration profile rather than water activity in MEA, especially in the PEM region. In order to get the water concentration profile in MEA, the interfacial boundary condition between gas diffusion layer and catalyst layer is necessary.

In this paper, the water concentration profile is directly solved and water content is taken based on the calculated water concentration. Also, current density is numerically predicted and compared with experimental data.

MATHEMATICAL MODEL

Fig. 1 shows a system schematic of a two dimensional PEM Fuel Cell. Whole governing equation is solved simultaneously in all seven layers by finite volume method. However, there is a phenomenally discontinuous distribution of numerical solution in the system. That is,

1. Hydrogen mass fraction (or mole fraction) exists only in ACH, AGDL, ACL
2. Oxygen mass fraction (or mole fraction) exists only in CCH, CGDL, CCL
3. Water mass fraction (or mole fraction) does not exist in ACL, PEM, CCL (MEA)
4. Water concentration exists only in ACL, PEM, CCL (MEA)
5. Electrolyte potential exists only in ACL, PEM, CCL (MEA)

There are several numerical techniques such as source term maximization, diffusion coefficient maximization to solve these discontinuous phenomena. Numerically, these techniques are for minimizing convection and diffusion effects in each governing equation. So, to some extent, there is a numerical error in the computational domain. However, if an interfacial boundary condition is added between the gas diffusion layer and catalyst layer, we can perfectly protect numerical diffusion and also the boundary condition setting of water concentration at ACL and CCL is possible.

Though, actually, all governing equations are solved simultaneously, phenomenally-calculated governing equations are different in each layer. So, for better understanding, mathematical models are overlapped in each layer.

1. Governing Equations

1-1. Anode Flow Channel (ACH)

In this paper we do not consider reforming processes and assume that only pure hydrogen gas is used as fuel. So, in the anode flow channel, humidified hydrogen gas is supplied. Mass fractions of two species (hydrogen, water vapor) are calculated by solving the species transport equation. Phenomenally, there are fluid convection and molecular diffusion in the channel. There are no source terms in each governing equation since the flow channel is not a porous medium and there are no electrochemical reactions.

$$\nabla\cdot(\varepsilon\rho_a^{eff}\vec{u})=0 \tag{1}$$

$$\nabla\cdot(\varepsilon\rho_a^{eff}\vec{u}\vec{u})=-\varepsilon\nabla p+\nabla\cdot(\varepsilon\rho_a^{eff}\nabla\vec{u}) \tag{2}$$

$$\nabla\cdot(\varepsilon\rho_a^{eff}\vec{u}\omega_{H_2})=\nabla\cdot(\varepsilon\rho_a^{eff}D_{H_2,g}\nabla\omega_{H_2}) \tag{3}$$

$$\nabla\cdot(\varepsilon\rho_a^{eff}\vec{u}\omega_{H_2O,g})=\nabla\cdot(\varepsilon\rho_a^{eff}D_{H_2O,g}\nabla\omega_{H_2O,g}) \tag{4}$$

where, ρ_a^{eff} is an effective fluid density based on species mixing and μ_a^{eff} means effective fluid viscosity. They are defined based on mass fraction ratio. Subscript "a" means anode.

$$\rho_a^{eff}=\frac{1}{\sum_i\frac{\omega_i}{\rho_i}} \tag{5}$$

$$\mu_a^{eff}=\sum_i\omega_i\cdot\mu_i \tag{6}$$

Also ε is unity since concept of porosity or volume fraction is unnecessary in this layer.

1-2. Anode Gas Diffusion Layer (AGDL)

In this region, ε value is valid. ε is a kind of concept of volume fraction, in other words, how much amount is taken by targeted volume out of total volume. Thus, when momentum conservation and species transport equation are considered in porous media, fluid volume fraction comes to be so-called porosity. All equations were formulated based on volume-averaged velocity concept. Darcy's law was used to describe momentum sink term and pore distribution in G.D.L. is assumed to be homogeneous. Source term, S_u, is defined in Table 1.

$$\nabla\cdot(\varepsilon_{a,GDL}\rho_a^{eff}\vec{u})=0 \tag{6}$$

$$\nabla\cdot(\varepsilon_{a,GDL}\rho_a^{eff}\vec{u}\vec{u})=-\varepsilon_{a,GDL}\nabla p+\nabla\cdot(\varepsilon_{a,GDL}\mu_a^{eff}\nabla\vec{u})+S_u \tag{7}$$

$$\nabla\cdot(\varepsilon_{a,GDL}\rho_a^{eff}\vec{u}\omega_{H_2})=\nabla\cdot(\varepsilon_{a,GDL}\rho_a^{eff}D_{H_2,g}\nabla\omega_{H_2}) \tag{8}$$

$$\nabla\cdot(\varepsilon_{a,GDL}\rho_a^{eff}\vec{u}\omega_{H_2O,g})=\nabla\cdot(\varepsilon_{a,GDL}\rho_a^{eff}D_{H_2O,g}\nabla\omega_{H_2O,g}) \tag{9}$$

1-3. Anode Catalyst Layer (ACL)

In this region, only molecular diffusion is considered since the fluid convection effect in catalyst layer is negligible. In this layer, the electron-conductive solid phase (platinum), proton-conductive electrolyte phase (ionomer) and gas-diffusible fluid phase co-exist. In each phase, different physical phenomena occur: (i) hydrogen gas diffuses from fluid phase into electrolyte phase (ionomer) to

Table 1. Sources of terms for each equation in each layer

	S_u (momentum)	S_i (species)	S_Φ (potential)
AGDL	$-\frac{\mu_a^{eff}}{K}\varepsilon_{AGDL}^2\vec{u}$	0	0
ACL	0	$-\frac{M_{H_2}}{2F}j_a, -\frac{M_{H_2O}}{2F}j_c - \nabla\cdot\left(\frac{n_d M_{H_2O}}{F}\vec{I}\right)$	$aj_{0,a}^{ref}\left(\frac{X_{H_2}}{X_{H_2,ref}}\right)^{1/2}\left[\exp\left(\frac{\alpha_a F}{RT}\cdot\eta_a\right)-\exp\left(\frac{\alpha_c F}{RT}\cdot\eta_a\right)\right]$
PEM	0	$-\nabla\cdot\left(\frac{n_d M_{H_2O}}{F}\vec{I}\right)$	0
CCL	0	$\frac{M_{O_2}}{4F}j_c, -\frac{M_{H_2O}}{2F}j_c - \nabla\cdot\left(\frac{n_d M_{H_2O}}{F}\vec{I}\right)$	$-aj_{0,c}^{ref}\left(\frac{X_{O_2}}{X_{O_2,ref}}\right)\left[\exp\left(\frac{\alpha_a F}{RT}\cdot\eta_c\right)-\exp\left(-\frac{\alpha_c F}{RT}\cdot\eta_c\right)\right]$
CGDL	$-\frac{\mu_c^{eff}}{K}\varepsilon_{CGDL}^2\vec{u}$	0	0

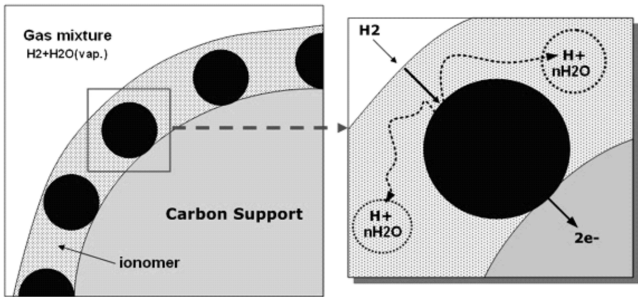

Fig. 2. Hydrogen gas diffusion mechanism in catalyst layer.

make an electrochemical reaction (see Fig. 2). (ii) water diffuses by concentration gradient in electrolyte phase. (iii) water migrates by potential gradient in electrolyte phase. (iv) electrolyte-phase potential exists in electrolyte phase. and (v) solid-phase potential exists in solid phase (e.g., platinum, graphite).

$$\nabla\cdot[\varepsilon_{e,cat}^{1.5}\rho_a^{eff}D_{H_2,m}\nabla\omega_{H_2}]+\varepsilon_{e,cat}S_{H_2}=0 \quad (10)$$

$$\nabla\cdot[\varepsilon_{e,cat}^{1.5}D_{H_2O,m}\nabla C_{H_2O,l}]=0 \quad (11)$$

$$\nabla\cdot[\varepsilon_{e,cat}^{1.5}\kappa_e\nabla\Phi_{e,a}]+\varepsilon_{e,cat}S_{\Phi,a}=0 \quad (12)$$

Especially the electrolyte-phase and solid-phase potential are phenomenally related to proton conduction and electron, respectively. In other words, the potential gradient in solid phase is a driving force for electron conduction and potential gradient in electrolyte phase is a driving force for proton conduction.

This means that there are solid phase potential value and electrolyte phase potential value in one control volume simultaneously (see Fig. 3) and thus the concept of volume fraction is introduced in order to handle this physical phenomenon. These two potential values are mathematically linked based on the definition of overpotential, $\eta=\Phi_s-\Phi_e-V_{oc}$. So, conceptually, two charge conservation equations have to be solved simultaneously. However, since solid-phase material (e.g., platinum, graphite) is highly electron-conductive, solid-phase potential is treated as a constant. In the charge conservation equation, the amount of charge generated in ACL is defined based on Butler-Volmer's equation and this equation is hydrogen mole fraction dependent. This means the species transport equation and charge conservation equation cannot be solved separately since variables in governing equations are tightly linked.

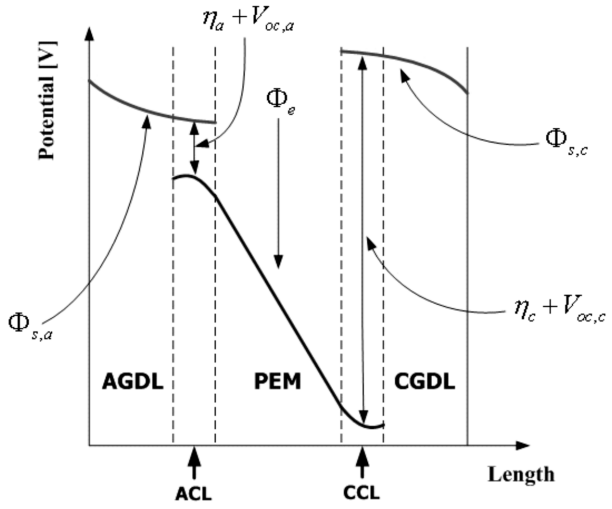

Fig. 3. Conceptual plot of phase potential distribution.

Also, the mole fraction of each species is calculated as below.

$$X_i=\frac{\frac{\omega_i}{M_i}}{\sum\frac{\omega_i}{M_i}} \quad (13)$$

1-4. Proton Exchange Membrane (PEM)

In this region molecular diffusion of water, water migration and proton conduction are considered. Also, it is assumed there is no momentum transfer through the whole membrane phase. The major driving force for proton migration is the electrolyte-phase potential gradient due to electrochemical reaction in the anode and cathode catalyst layer.

$$\nabla\cdot[\varepsilon_{H_2O,m}^{1.5}D_{H_2O,m}\nabla C_{H_2O,l}]=0 \quad (14)$$

$$\nabla\cdot[\varepsilon_{e,m}^{1.5}\kappa_e\nabla\Phi_e]=0 \quad (15)$$

1-5. Cathode Catalyst Layer (CCL)

The concept and numerical treatment are basically identical with anode catalyst layer (ACL); only sort of the species is different.

$$\nabla\cdot[\varepsilon_{e,cat}^{1.5}\rho_c^{eff}D_{O_2,m}\nabla\omega_{O_2}]+\varepsilon_{e,cat}S_{O_2}=0 \quad (16)$$

$$\nabla\cdot[\varepsilon_{e,cat}^{1.5}D_{H_2O,m}\nabla C_{H_2O,l}]+\varepsilon_{e,cat}S_{H_2O,l}=0 \quad (17)$$

Table 2. Boundary conditions for momentum conservations equation and scalar transport equations

	Momentum	ω_{H_2}	ω_{O_2}	$\omega_{H_2O,G}$	$C_{H_2O,L}$	Φ_e
B.C.01	$\frac{\zeta_a}{X^a_{H_2,in}}\frac{I_{ref}}{2F}\frac{RT_{in,a}}{P_{in,a}}\frac{A_{MEA}}{A_{ch,a}}$	specified value	$\omega_{O_2}=0$	specified value	$C_{H_2O,l}=0$	$\Phi_e=0$
B.C.02	$\frac{\zeta_c}{X^c_{O_2,in}}\frac{I_{ref}}{4F}\frac{RT_{in,c}}{P_{in,c}}\frac{A_{MEA}}{A_{ch,c}}$	$\omega_{H_2}=0$	specified value	specified value	$C_{H_2O,l}=0$	$\Phi_e=0$
B.C.03	specifies value	$\frac{\partial\omega_{H_2}}{\partial y}=0$	$\frac{\partial\omega_{O_2}}{\partial y}=0$	$\frac{\partial\omega_{H_2O,g}}{\partial y}=0$	$\frac{\partial C_{H_2O,l}}{\partial y}=0$	$\frac{\partial\Phi_e}{\partial y}=0$
B.C.04	specifies value	$\frac{\partial\omega_{H_2}}{\partial y}=0$	$\frac{\partial\omega_{O_2}}{\partial y}=0$	$\frac{\partial\omega_{H_2O,g}}{\partial y}=0$	$\frac{\partial C_{H_2O,L}}{\partial y}=0$	$\frac{\partial\Phi_e}{\partial y}=0$
B.C.09	$\frac{\partial u}{\partial x}=0$	$D\frac{\partial\omega_{H_2}}{\partial x}\Big\vert_{AGDL}=D\frac{\partial\omega_{H_2}}{\partial x}\Big\vert_{ACL}$	$\frac{\partial\omega_{O_2}}{\partial x}=0$	$\frac{\partial\omega_{H_2O,g}}{\partial x}=0$	$\frac{\rho_{m,dry}\omega_{H_2O,g}}{M_{H_2O}}\times\varepsilon_{H_2O,m}$	$\frac{\partial\Phi_e}{\partial x}=0$
B.C.10	$\frac{\partial u}{\partial x}=0$	$\frac{\partial\omega_{H_2}}{\partial x}=0$	$D\frac{\partial\omega_{O_2}}{\partial x}\Big\vert_{CCL}=D\frac{\partial\omega_{O_2}}{\partial x}\Big\vert_{CGDL}$	$\frac{\partial\omega_{H_2O,g}}{\partial x}=0$	$\frac{\rho_{m,dry}\omega_{H_2O,g}}{M_{H_2O}}\times\varepsilon_{H_2O,m}$	$\frac{\partial\Phi_e}{\partial x}=0$

(Note!) Boundary conditions for all scalar variables at from B.C.05 to B.C.08 are set as non-flux.

$$\nabla\cdot[\varepsilon_{e,cat}^{1.5}\kappa_e\nabla\Phi_{e,c}]+\varepsilon_{e,cat}S_{\Phi,c}=0 \quad (18)$$

1-6. Cathode Gas Diffusion Layer (CGDL)

The concept and numerical treatment are basically identical with anode gas diffusion layer (AGDL); only sort of the species is different.

$$\nabla\cdot(\varepsilon_{c,GDL}\rho_c^{eff}\vec{u})=0 \quad (19)$$

$$\nabla\cdot(\varepsilon_{c,GDL}\rho_c^{eff}\vec{u}\vec{u})=-\varepsilon_{c,GDL}\nabla p+\nabla\cdot(\varepsilon_{c,GDL}\mu_c^{eff}\nabla\vec{u})+S_u \quad (20)$$

$$\nabla\cdot(\varepsilon_{c,GDL}\rho_c^{eff}\vec{u}\omega_{O_2})=\nabla\cdot(\varepsilon_{c,GDL}\rho_c^{eff}D_{O_2,g}\nabla\omega_{O_2}) \quad (21)$$

$$\nabla\cdot(\varepsilon_{c,GDL}\rho_c^{eff}\vec{u}\omega_{H_2O,g})=\nabla\cdot(\varepsilon_{c,GDL}\rho_c^{eff}D_{H_2O,g}\nabla\omega_{H_2O,g}) \quad (22)$$

1-7. Cathode Flow Channel (CCH)

The concept and numerical treatment are basically identical with anode flow channel (ACH); only sort of the species is different.

$$\nabla\cdot(\rho_c^{eff}\vec{u})=0 \quad (23)$$

$$\nabla\cdot(\rho_c^{eff}\vec{u}\vec{u})=-\nabla p+\nabla\cdot(\mu_c^{eff}\nabla\vec{u}) \quad (24)$$

$$\nabla\cdot(\rho_c^{eff}\vec{u}\omega_{O_2})=\nabla\cdot(\rho_c^{eff}D_{O_2,g}\nabla\omega_{O_2}) \quad (25)$$

$$\nabla\cdot(\rho_c^{eff}\vec{u}\omega_{H_2O,g})=\nabla\cdot(\rho_c^{eff}D_{H_2O,g}\nabla\omega_{H_2O,g}) \quad (26)$$

Though two species transport equations are also considered at the cathode compartment, there are actually three kinds of species (e.g. O_2, H_2O, N_2). However we do not have to solve whole three governing equations since the mass fraction of nitrogen can be gained by $1-(\omega_{H_2}+\omega_{H_2O})$ at each control volume.

2. Boundary Conditions

In Fig. 1, boundary symbols are designated at each boundary. At the anode and cathode inlet boundary (B.C.01 & B.C.02), the velocity boundary condition is given based on stoichiometry, u=f(ζ, X_i, I_{ref}, P_{in}, T_{in}, A_{MEA}, A_{ch}). At the anode and cathode outlet boundary, the pressure values for the momentum conservation equation are given as a boundary condition. This is because operating pressure values are usually experimentally measured at the outlet. Additionally, for other scalar transport equations, non-flux boundary condition was used.

At interfacial boundaries between the gas diffusion layer and catalyst layer, basically wall-type boundary condition was used. By giving this boundary into the interfacial region, seven layers are conceptually divided into three computational domains: (i) ACH, ADGL region, (ii) ACL, PEM, CCL region, and (iii) CGDL, CCH region.

The main purpose for using this interfacial boundary condition is to give boundary conditions for water concentration and charge conservation equation. Also, because of this boundary condition, it is easier to solve charge conservations equation since numerical diffusion from catalyst layer to gas diffusion layer is perfectly blocked.

Additionally, since a wall-type boundary condition is used at B.C.09 and B.C.10, species diffusion through this boundary is numerically impossible. In order to solve this, the flux-coupling method for H_2, O_2, H_2O(vap.) equations is used.

More specific mathematical expressions for each boundary are presented in Table 2.

3. Water Transport in MEA

Fig. 4 shows the water transport mechanism introduced in this paper. Typically, there are several important physical phenomena to explain water transport in membrane:

(i) water generation in cathode catalyst layer
(ii) molecular diffusion by concentration gradient
(iii) migration by electrolyte-potential gradient
(iv) migration by capillary force

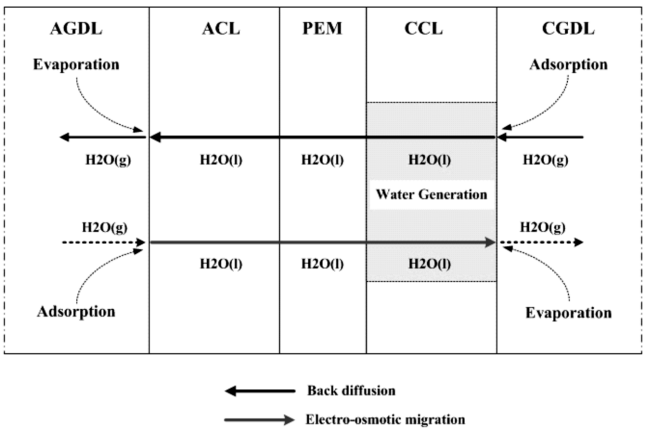

Fig. 4. Conceptual approach for describing water transport in MEA.

The current model in this paper covers (i), (ii) and (iii) since (i), (ii) and (iii) are the most influential effects in water transport. It is simply assumed that gas phase water (water vapor) is condensed into ACL and CCL through the interfacial boundary between the gas diffusion layer and catalyst layer. Thus condensed water vapor is thought to be adsorbed into membrane. Absorbed water is considered as liquid phase and physical properties for the water concentration equation are used based on liquid phase water.

Though it is not included in this paper, water state in MEA is very important in macroscopic modeling. In order to solve molecular diffusion in MEA, using appropriate physical properties is necessary. According to Adam's research [2003], the water state in membrane is water-content-dependent; thus there is a transient phase between gas phase and liquid phase. In order to deal with this physical situation, a more reliable mathematical expression is needed. For one example, the density of gas phase water and liquid phase water is extremely different. So, from this point of view, dealing with the physical state of water might be very important.

4. Current Density Calculation

Once electrolyte-phase potential values in each control volume are calculated, it is possible to calculate the phase-potential gradient in MEA. Also, we know the proton conductivities in each control volume. So, current density and current density magnitude calculation are performed as presented below in each control volume.

$$\vec{I} = -\kappa_e\left(\frac{\partial \Phi_e}{\partial x}\vec{i} + \frac{\partial \Phi_e}{\partial y}\vec{j}\right) \tag{27}$$

$$|\vec{I}| = \kappa_e\sqrt{\left(\frac{\partial \Phi_e}{\partial x}\right)^2 + \left(\frac{\partial \Phi_e}{\partial y}\right)^2} \tag{28}$$

Additionally, the average current density value in MEA is determined by

$$|\vec{I}|_{avg} = \frac{1}{A}\int |\vec{I}|\,dA \tag{29}$$

5. Numerical Implementation

In this paper, numerical modeling and simulation of two dimensional PEMFC were implemented with commercially-available CFD code, FLUENT. However, since FLUENT does not present an electrochemistry modeling module, whole governing equations except momentum conservation equation were solved by using User-Defined Functions, a kind of user subroutine program.

In the case of charge conservation equation, source terms are tightly linked with species transport equations. Also, comparably quite low under-relaxation factors and proper convergence criteria were used for stable convergence since slope of those source terms are numerically very stiff.

Over 200,000 iterations were taken to reduce each residual value below 10^{-6} and make numerical solutions stabilized. Especially, even though species transport equations and charge conservation equations are converged to some degree, more iterations are needed to make current density values well-converged. This is because current density values in each control volume are so sensitively affected by the slope of potential profile.

Choosing proper under-relaxation factors can sometimes reduce computation time dramatically since the number of iterations is generally affected by under-relaxation factors. In this paper, since the value of under-relaxation factors is very low (e.g. 0.001), a huge number of iterations were required.

A 50×180 (9,000 cells) mesh system was used in all simulation cases for the sake of fast convergence. Computation time per each case requires over 24 hours.

RESULTS AND DISCUSSIONS

Figs. 5 and 6 show hydrogen and oxygen mole fraction distribution in ACL and CCL, respectively. Phenomenally, the amount and distribution of hydrogen gas and oxygen gas are among the most important factors in determining electrolyte-phase potential field. In other words, the electrolyte-phase potential in ACL is generated by hydrogen oxidation reaction and that in CCL is depleted by oxygen reduction reaction. Theoretically, in ideal state, amount of charge generated in ACL and the amount of current depleted in CCL are exactly same. Numerically, generation and depletion are treated as source terms in each governing equation.

As it is shown in Figs. 5 and 6, electrolyte-phase potential values

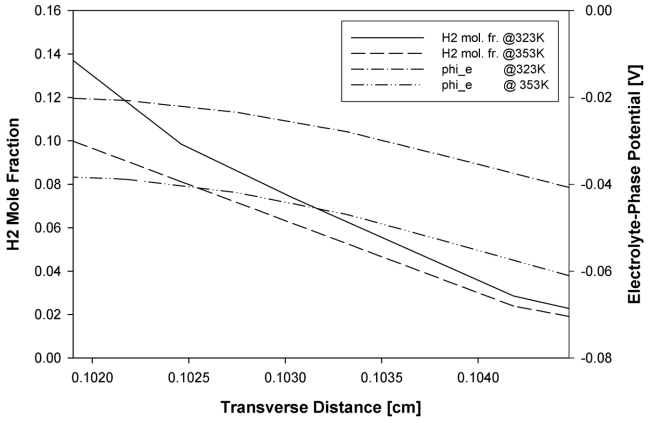

Fig. 5. Hydrogen mole fraction and electrolyte-phase potential distribution in anode catalyst layer (ACL) along x-directional transverse distance at y=3.556 cm (1/2 L) when W_{cell}=0.6 V, P_a=3 atm, P_c=5 atm, T_{cell}=323 K & 353 K, ζ_a=2.8, ζ_c=3.0.

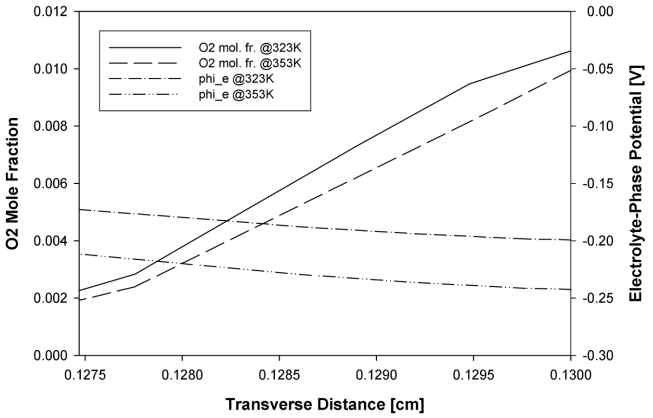

Fig. 6. Oxygen mole fraction and electrolyte-phase potential distribution in cathode catalyst layer (CCL) along x-directional transverse distance at y=3.556 cm (1/2 L) when W_{cell}=0.6 V, P_a=3 atm, P_c=5 atm, T_{cell}=323 K & 353 K, ζ_a=2.8, ζ_c=3.0.

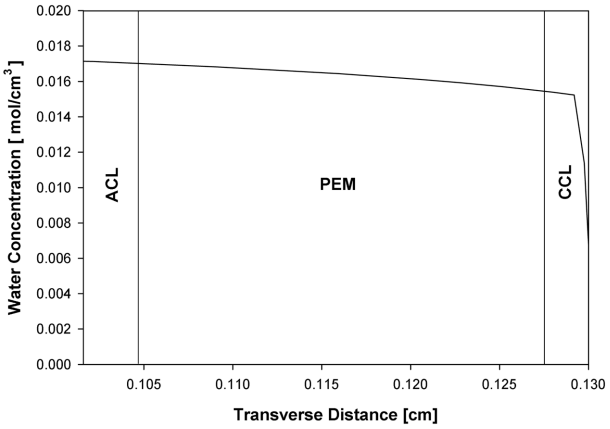

Fig. 7. Water concentration distribution in MEA along x-directional transverse distance at y=3.556 cm (1/2 L) when W_{cell}=0.6 V, P_a=3 atm, P_c=5 atm, T_{cell}=353 K, ζ_a=2.8, ζ_c=3.0.

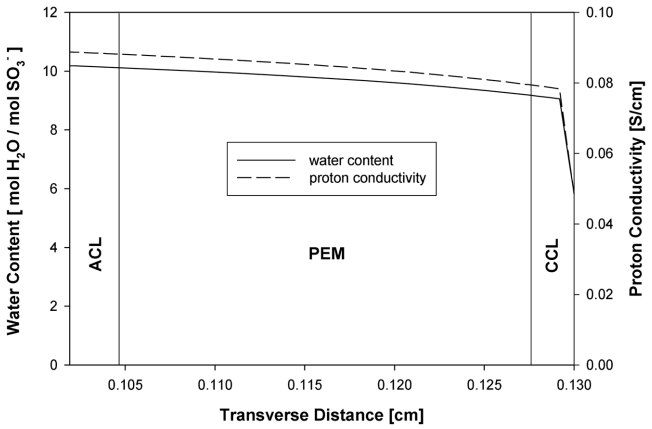

Fig. 8. Water content and proton conductivity distribution in MEA along x-directional transverse distance at y=3.556 cm (1/2 L) when W_{cell}=0.6 V, P_a=3 atm, P_c=5 atm, T_{cell}=353 K, ζ_a=2.8, ζ_c=3.0.

are affected by cell temperature and mole fraction of fuel gas. In this case, it is not easy to single out the specific reason for electrolyte-phase potential distribution since the potential value is determined by mixed effects. Moreover, according to Table 1, generation and depletion of electrolyte-phase potential are affected by H_2 mole fraction, O_2 mole fraction, cell temperature and even electrolyte potential itself. However, in the case of Figs. 5 and 6, since inlet boundary conditions are equal to each other, only cell temperature is a key factor in differentiating electrolyte-phase potential values in MEA, and the results show generation and depletion of electrolyte-phase potential are inversely proportional to the cell temperature. So, due to the different cell temperature, the reaction rate in ACL and CCL is different, and consequently the mole fraction of hydrogen and oxygen in each case is different.

Fig. 7 shows the water concentration profile in MEA. In this paper, it was assumed that water vapor is condensed into liquid water at an interface of gas diffusion layer and catalyst layer (see Fig. 1 and Table 2) and the state of water in MEA is liquid. The concept of water concentration is different in that solvent is not solid phase and solute is liquid water. From this point of view, water concentration in MEA can be considered as a kind of distribution of the amount of liquid water. A sharp drop in CCL region is due to operating condition since there is no humidification process in the cathode compartment. Though there is a water generating reaction in CCL, the water concentration profile is different from the normal case, i.e., the general water concentration profile has a peak point in CCL and molecular diffusion by concentration gradient takes

Table 3. Physical properties and parameters

Property	Value
H_2 diffusion coeff. in gas phase [m^2/s]	$1.1\times10^{-4}\left(\frac{T}{353}\right)^{3/2}\left(\frac{1}{p}\right)$
H_2 diffusion coeff. in electrolyte [m^2/s]	2.59×10^{-10}
O_2 diffusion coeff. in gas phase [m^2/s]	$3.5\times10^{-5}\left(\frac{T}{353}\right)^{3/2}\left(\frac{1}{p}\right)$
O_2 diffusion coeff. in electrolyte [m^2/s]	1.22×10^{-10}
H_2O diffusion coeff. in gas phase [m^2/s]	$7.35\times10^{-5}\left(\frac{T}{353}\right)^{3/2}\left(\frac{1}{p}\right)$
H_2O diffusion coeff. in electrolyte [m^2/s]	$\begin{cases} 3.1\times10^{-7}\cdot\lambda\cdot(e^{0.28\lambda}-1)\cdot e^{-2346/T} & \text{for } 0<\lambda<3 \\ 4.17\times10^{-8}\cdot\lambda\cdot(1+161\times e^{\lambda})\cdot e^{-2346/T} & \text{other ranges} \end{cases}$
Proton conductivity [s/m]	$(0.5139\lambda-0.326)\exp\left[1268\left(\frac{1}{303}-\frac{1}{T}\right)\right]$
Water content	$\frac{M_{m,dry}}{\rho_{m,dry}}\times C_{H_2O,L}$
Cell temperature [K]	353
Anode operating pressure [Pa]	303975
Cathode operating pressure [Pa]	506625
Anode stoichiometry	2.8
Cathode stoichiometry	3.0

place from CCL to ACL. However, this is totally operating-condition-dependent. Thus, according to the operating condition, a peak value in water concentration may exist in ACL. In the case of Fig. 7, as mentioned above, there is no humidification process at the cathode compartment. So, if the amount of water is comparably abundant at CCL, the peak value of water concentration can be in CCL.

Fig. 8 shows water content and proton conductivity profile in MEA. As it is shown in Table 3, the water concentration, water content and proton conductivity are physically and mathematically linked with each other. Mathematically, water content is a function of water concentration and proton conductivity is a function of water content. So the shape of each graph is very similar.

Figs. 9 and 10 show anode and cathode over-potential profile in ACL and CCL. In this paper, though open-circuit potential is a function of temperature, since isothermal operating condition is assumed, it is a kind of constant value. Solid-phase potential in ACL and CCL is also a constant since we do not solve the solid-phase phase potential equation under an assumption that solid-phase material is highly electron-conductive; thus there is no potential gradient. Based on the definition of over-potential, $\eta=\Phi_s-\Phi_e-V_{oc}$, anode and cathode over-potentials are function of electrolyte-phase potential. When electrolyte-phase potential profiles in Figs. 5 and 6 are considered, the anode and cathode over-potential profiles in Figs. 9 and 10 can be considered to be properly predicted.

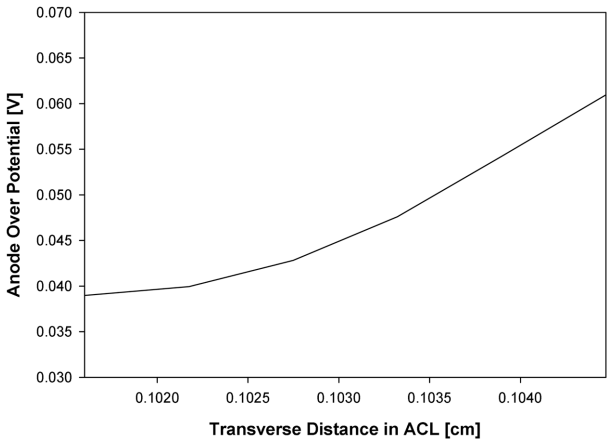

Fig. 9. Anode over-potential distribution along x-directional transverse distance at y=3.556 cm (1/2 L) when W_{cell}=0.6 V, P_a= 3 atm, P_c=5 atm, T_{cell}=353 K, ζ_a=2.8, ζ_c=3.0.

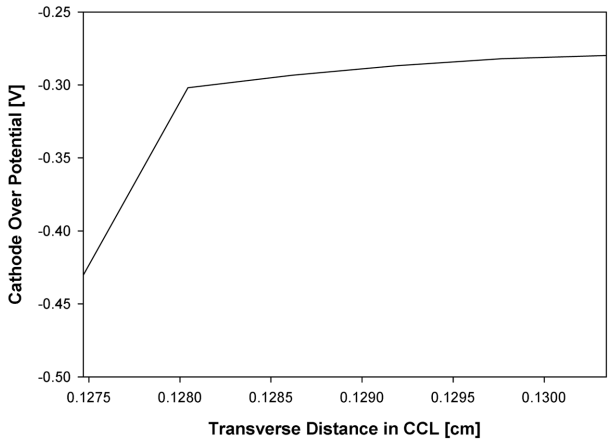

Fig. 10. Cathode over-potential distribution along x-directional transverse distance at y=3.556 cm (1/2 L) when W_{cell}=0.6 V, P_a=3 atm, P_c=5 atm, T_{cell}=353 K, ζ_a=2.8, ζ_c=3.0.

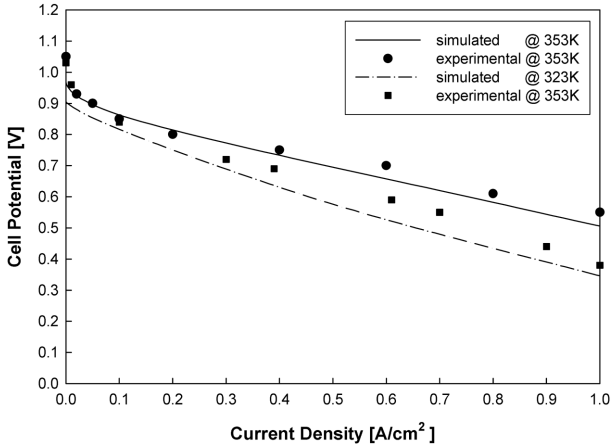

Fig. 11. Comparison of simulated and measured polarization curve @ P_a=3 atm, P_c=5 atm, T_{cell}=323 K & 353 K, ζ_a=2.8, ζ_c=3.0.

Fig. 11 shows a result comparison between experimental and simulated data. Experimental data were taken from Ticianelli's [1988] paper. Each data point stands for averaged-value through MEA. As it is shown, the current mathematical model slightly under-predicts current density value at a given cell potential and needs to be modified to describe more detailed phenomena. However, in a general manner, our model and approaching methodology are quite reasonable for predicting water concentration profile directly.

CONCLUSIONS

A two dimensional, isothermal and steady-state PEMFC model was developed by using a unique numerical technique. To directly calculate the water concentration profile in MEA, we firstly introduced an interfacial boundary condition into the interface between gas diffusion layer (GDL) and catalyst layer (CL) and also attained physically reasonable data.

More specific physical phenomena such as water state in MEA, temperature-changing situation should be considered for more realistic model development and we are currently focusing on these topics.

NOMENCLATURE

A : surface area [m^2]
ACH : anode flow channel
AGDL : anode gas diffusion layer
ACL : anode catalyst layer
C : molar concentration [kgmol/m^3]
CCH : cathode flow channel
CGDL : cathode gas diffusion layer
CCL : cathode catalyst layer
D : mass diffusion coefficient [m^2/s]
F : Faraday constant [C/kgmol]
I : current density [A/m^2]
j : volumetric current flow [A/m^3]

L : hydraulic permeability [m^2]
M : molecular weight (or equivalent weight) [kg/kgmol]
n_d : electro-osmotic drag coefficient
P : pressure [Pa]
PEM : proton exchange membrane
T : temperature [K]
u : velocity vector
V_{oc} : open-circuit voltage
X : mole fraction

Greek Letters

α : transfer coefficient
ε : fluid porosity (or volume fraction)
λ : water content [mol H_2O/mol SO_3^-]
ρ : density [kg/m^3]
μ : viscosity [kg/m·s]
ω : mass fraction
κ_e : proton conductivity [S/m]
Φ : phase potential [V]
ζ : stoichiometry

Subscripts

a : anode
c : cathode
ch : channel
cat : catalyst phase
e : electrolyte phase
g : gas phase
in : inlet
l : liquid phase
m : membrane phase
MEA : membrane electrode assembly
ref : reference value
s : solid phase

Superscripts

a : anode
c : cathode
eff : effective value

REFERENCES

Bernadi, D. M. and Verbrugge, M. W., "Mathematical Model of a Gas Diffusion Electrode Bonded to a Polymer Electrolyte," *AIChE J.*, **37**(8), 1151 (1991).

Berning, T., Lu, D. M. and Djilali, N., "Three-dimensional Computational Analysis of Transport Phenomena in PEM Fuel Cell," *J. Power Sources*, **106**, 284 (2002).

Bird, R. B., Stewart, W. E. and Lightfoot, E. N., "Transport Phenomena," John Wiley & Sons, Inc. (1960).

Carrette, L., Friedrich, K. A. and Stimming, U., "Fuel Cells-Fundamentals and Applications," *FUEL CELLS*, **1**, 5 (2001).

Carrette, L., et al., "Fuel Cells: Principles, Types, Fuels, and Applications," *CHEMPHYSCHEM*, **1**, 162 (2000).

Center for Fuel Cell Research at USC : http://www.che.sc.edu/centers/PEMFC

CFD Online : http://www.cfd-online.com

Choi, K.-H., Peck, D. H., Kim, C. S., Shin, D. R. and Lee, T. H., "Water Transport in Polymer Membranes for PEMFC," *J. Power Sources*, **86**, 197 (2000).

Davis, C. W., "A Dictionary of Electrochemistry," THE MACMILLAN PRESS Ltd. (1976).

DuPont's Web Site : http://www.dupont.com

Dutta, S., Shimpalee, S. and Van Zee, J. W., "Three-dimensional Numerical Simulation of Straight Channel PEM Fuel Cells," *J. Appl. Electrochem.*, **30**, 135 (2000).

Electrochemical Engine Center at Penn State University : http://mtrl1.me.psu.edu

"High Temperature Membranes for Solid Polymer Fuel Cells," ETSU F/02/00189/REP (2001).

Himmelblau, D. M., "Basic Principles and Calculations in Chemical Engineering," Prentice-Hall International, Inc. (1996).

IESVic Integrated Energy Systems : http://www.iesvic.uvic.ca

Jo, J. H., "A Mathematical Modeling of an Alkaline Fuel Cell," Ph.D. Dissertation, Hanyang University (1999).

Kordesch, K. and Simader, G., "Fuel Cells and Their Applications," VCH (1996).

Korea Fuel Cell Community : http://www.freechal.com/fuelcell

Larminie, J., "Fuel Cell Systems Explained," JOHN WILEY & SONS LTD. (2000).

Module 4 : Fuel Cell Technology, Hydrogen Fuel Cell Engines and Related Technologies, College of the Desert (2001).

Patankar, S. V., "Numerical Heat Transfer and Fluid Flow," Hemisphere Publishing Corporation (1980).

Singh, D., Lu, D. M. and Djilali, N., "A Two-dimensional Analysis of Mass Transport in Proton Exchange Membrane Fuel Cells," *Int. J. Eng. Sci.*, **37**, 431 (1999).

Springer, T. E., Zawodzinski, T. A. and Gottesfeld, S., "Polymer Electrolyte Fuel Cell Model," *J. Electrochem. Soc.*, **138**(8), 2334 (1991).

Srinivasan, S., Manko, D. J., Koch, H., Enayetullah, M. A. and Appleby, A. J., "Recent Advances in Solid Polymer Electrolyte Fuel Cell Technology with Low Platinum Loading Electrodes," *J. Power Sources*, **29**, 367 (1990).

Um, S. K., Wang, C. Y. and Chen, K. S., "Computational Fluid Dynamics Modeling of Proton Exchange Membrane Fuel Cells," *J. Electrochem. Soc.*, **147**(12), 4485 (2000).

Wang, C. Y. and Gu, W. B., "Micro-macroscopic Coupled Modeling of Battery and Fuel Cell Systems. Part II: Application to Ni-Cd and Ni-MH Cells," *J. Electrochem. Soc.*, **145**(10), (1998).

Weber, A. Z. and Newman, J., "Transport in Polymer-Electrolyte Membranes: I. Physical Model," *J. Electrochem. Soc.*, **150**(7), A1008 (2003).

White, R. E., Lorimer, S. E. and Darby, R., "Prediction of the Current Density at an Electrode at Which Multiple Electrode Reactions Occur under Potentiostatic Control," *J. Electrochem. Soc.*, **130**, 1123 (1983).